JOURNAL OF PETROLOGY | VOLUME 0 | NUMBER 0 | PAGES 1–14 | 2011 | doi:10.1093/petrology/egq093
Journal of Petrology Advance Access published February 8, 2011

Oceanic Volcanism from the Low-velocity Zone – without Mantle Plumes

DEAN C. PRESNALL[1,2] AND GUDMUNDUR H. GUDFINNSSON[2,3]

[1]DEPARTMENT OF GEOSCIENCES, UNIVERSITY OF TEXAS AT DALLAS, PO BOX 830688, RICHARDSON, TX 75083-0688, USA

[2]BAYERISCHES GEOINSTITUT, UNIVERSITÄT BAYREUTH, D-95447 BAYREUTH, GERMANY

[3]ICELAND GEOSURVEY, GRENSASVEGUR 9, 108 REYKJAVIK, ICELAND

RECEIVED JULY 22, 2009; ACCEPTED DECEMBER 6, 2010

We develop a model for oceanic volcanism that involves fracturing of the seismic lithosphere to access melts from the partly melted seismic low-velocity zone. Data on global seismic shear-wave velocities are combined with major-element compositions of global mid-ocean ridge basalt glasses, Hawaiian basalt glasses, and phase relations in the CaO-MgO-Al_2O_3-SiO_2-CO_2 and CaO-MgO-Al_2O_3-SiO_2-Na_2O-FeO systems at pressures from 1 atm to 6 GPa. We use these data to constrain the pressure–temperature conditions for melt extraction at Hawaii and mid-ocean ridges (including Iceland), and to evaluate the existence of hot mantle plumes. In the low-velocity zone, the maximum reduction and maximum anisotropy of seismic shear-wave velocity (maximum melt fraction) occurs at a depth of ~140–150 km for crustal ages >~50 Ma, and a depth of ~65 km at the East Pacific Rise axis. Seismic data indicate a smooth depth transition between these extremes. Experimental phase-equilibrium data, when combined with natural glass compositions, show that pressure–temperature conditions of tholeiitic melt extraction at Hawaii (~4–5 GPa, 1450–1500°C) and the global oceanic ridge system (~1·2–1·5 GPa, 1250–1280°C) are an excellent match for the two depth ranges of maximum melting indicated by seismic shear-wave data. At Hawaii, magmas escape to the surface along a fracture system that extends through the lithosphere into the low-velocity zone. This allows eruption of progressively deeper melts from the low-velocity zone, which exist at equilibrium along a normal geotherm. No significant decompression melting occurs. This produces the characteristic sequence at each volcano of initial low-volume alkalic magmas, then voluminous tholeiitic magmas that show low-pressure olivine-controlled crystallization, and final low-volume alkalic magmas from extreme depths. At the East Pacific Rise, the more shallow depth of magma extraction is caused by a perturbed ridge geotherm that grazes the lherzolite solidus within the thermal boundary layer. This results in an absence of olivine-controlled crystallization. Hawaii is not a hot plume. Instead, it shows magmas characteristic of normal mature-ocean thermal conditions in the low-velocity zone. We find no evidence of anomalously high temperatures of magma extraction and no role for hot mantle plumes anywhere in the ocean basins.

KEY WORDS: *basalt; carbonate; CMAS; geotherm; low-velocity zone; mantle plume; MORB*

INTRODUCTION

We use a combination of natural basalt glass compositions compiled from the literature, experimental data on the melting behavior of model mantle systems, and seismic data on shear-wave velocities in the oceanic upper mantle to examine the origin of oceanic volcanism and the existence of hot mantle plumes (Morgan, 1971, 1972) beneath mid-ocean ridges and elsewhere in the ocean basins. Foulger *et al.* (2005*c*), Campbell & Kerr (2007), and Foulger & Jurdy (2007) have provided a thorough introduction to the plume literature. Anderson (2011) has provided a geophysical perspective on the plume issue. Sleep (2007) has estimated that mantle plumes require temperatures that are enhanced by ~250°C relative to their surroundings. To determine if temperature enhancements of this magnitude exist at Hawaii or along mid-ocean ridges where several plumes (e.g. Iceland,

*Corresponding author. E-mail: presnall@utdallas.edu

Easter Island, Afar) have been proposed, it is necessary to compare pressure-temperature (*P-T*) conditions of magma extraction with anticipated normal temperature conditions in the mantle. The Pacific Basin, with its large expanse of young to mature oceanic lithosphere that has been thoroughly characterized seismically, is the best oceanic region for determining the normal range of upper mantle temperatures versus lithospheric age. It provides an important reference state for determining if candidate plumes have sufficient excess temperature to satisfy the thermal requirement of Sleep (2007). It also contains the strongest plume candidate, Hawaii, as well as the most vigorous mid-ocean ridge, the East Pacific Rise. We also examine melt-extraction temperatures at Iceland, the strongest plume candidate along a mid-ocean ridge. We address *P–T* conditions of magma extraction by combining data on (1) basalt glass compositions from Hawaii, Iceland, and the global mid-ocean ridge system, (2) experimentally determined phase relations in model systems and natural compositions over a range of pressures from 1 atm to 6 GPa, and (3) seismic data on shear-wave velocity and shear-wave anisotropy versus depth in the upper oceanic mantle.

Our database of MORB glass compositions (Fig. 1) contains 391 analyses from Iceland (Nordic Volcanological Institute, unpublished data generously made available to us by K. Gronvold; Sigurdsson & Sparks, 1981; Condomines *et al.*, 1983; Meyer *et al.*, 1985; Risku-Norja, 1985; Trønnes, 1990; Hansteen, 1991; Werner, 1994; Gurenko & Chaussidon, 1995; Schiellerup, 1995; Sigurdsson *et al.*, 2000; Steinthórsson *et al.*, 2000; Breddam, 2002), 25 from the Siqueiros Fracture Zone (Perfit *et al.*, 1996), six from Macquarie Island (Kamenetsky & Maas, 2002) (six alkalic glasses deleted), and 6542 from the petDB database, http://www.petdb.org/petdbWeb/index.jsp (88 alkalic glasses deleted). The olivine-controlled glass compositions from Kilauea volcano, Hawaii are from Clague *et al.* (1995). The petDB glass analyses are filtered to retain only analyses classified as 'fresh' and sampled from spreading ridges and fracture zone segments that connect these ridges. Only compositions with totals between 98·5 and 101·5% are retained.

MELT-EXTRACTION TEMPERATURES BASED ON OLIVINE ADDITION

An understanding of magma extraction temperatures is critical to determining the existence of hot mantle plumes. To obtain this information, a number of recent efforts have used 'olivine-addition' calculations. These studies (Herzberg & O'Hara, 2002; Falloon *et al.*, 2005, 2007; Green & Falloon, 2005; Putirka, 2005, 2008; Courtier *et al.*, 2007; Herzberg *et al.*, 2007; Putirka *et al.*, 2007; Herzberg & Asimow, 2008; Lee *et al.*, 2009) have reported a wide range of calculated potential temperatures (T_p, the projected temperature at zero pressure of the adiabatic temperature gradient within the upper mantle) of 1286–1722°C at Hawaii, 1361–1637°C for Iceland, and 1243–1488°C for mid-ocean ridge basalts (MORB) exclusive of those at Iceland. For MORB, including those at Iceland, these studies assume the existence of olivine-controlled crystallization at low temperatures and pressures. For example, in the studies of Falloon *et al.* (2005, 2007), each calculated temperature is based on the occurrence of a highly magnesian olivine crystal that is out of equilibrium with its host glass. Olivine is then incrementally added back into the glass composition until its Mg/Fe ratio matches the expected Mg/Fe ratio of a melt in equilibrium with the observed olivine crystal. This procedure assumes that the liquid and crystal have existed as a closed system and that these phases were once in equilibrium at a high temperature of melt extraction. However, for magma extraction from a compositionally heterogeneous mantle, melts and crystals with a range of Mg/Fe ratios from different sources of varying fertility could be mixed. Model-system phase relations (Gudfinnsson & Presnall, 2000; Presnall & Gudfinnsson, 2008) show that in a heterogeneous mantle, formation of a melt with an extremely high Mg/Fe ratio from a correspondingly depleted lherzolitic source is consistent with melt extraction at the very low solidus temperatures and pressures of the plagioclase-spinel lherzolite transition (~1250–1280°C, 1·2–1·5 GPa). If an olivine crystal in equilibrium with such a highly depleted melt were swept up by a different and more fertile (lower Mg/Fe) melt in this same *P-T* range, the back-calculation to the presumed original equilibrium temperature for this disequilibrium crystal–liquid pair would indicate an elevated temperature unrelated to the low temperature at which this Mg-rich crystal grew in its previous environment. Because of the possibility of very large errors of this type and the inability to determine the magnitude of these errors, potential temperatures based on reconstructed magma compositions are not used here.

PHASE RELATIONS

In our determinations of the *P-T* conditions of magma extraction, we use model-system phase relations in conjunction with temperature adjustments to achieve natural conditions. In the system CaO-MgO-Al_2O_3-SiO_2 (CMAS), the forsterite (Mg_2SiO_4)-diopside ($CaMgSi_2O_6$)-anorthite ($CaAl_2Si_2O_8$)-silica (SiO_2) tetrahedron (Fig. 1a) is a close approximation of the tholeiitic portion of the basalt tetrahedron (Yoder & Tilley, 1962) for natural compositions and includes all the major silicate phases involved in tholeiitic melting and crystallization processes. In the

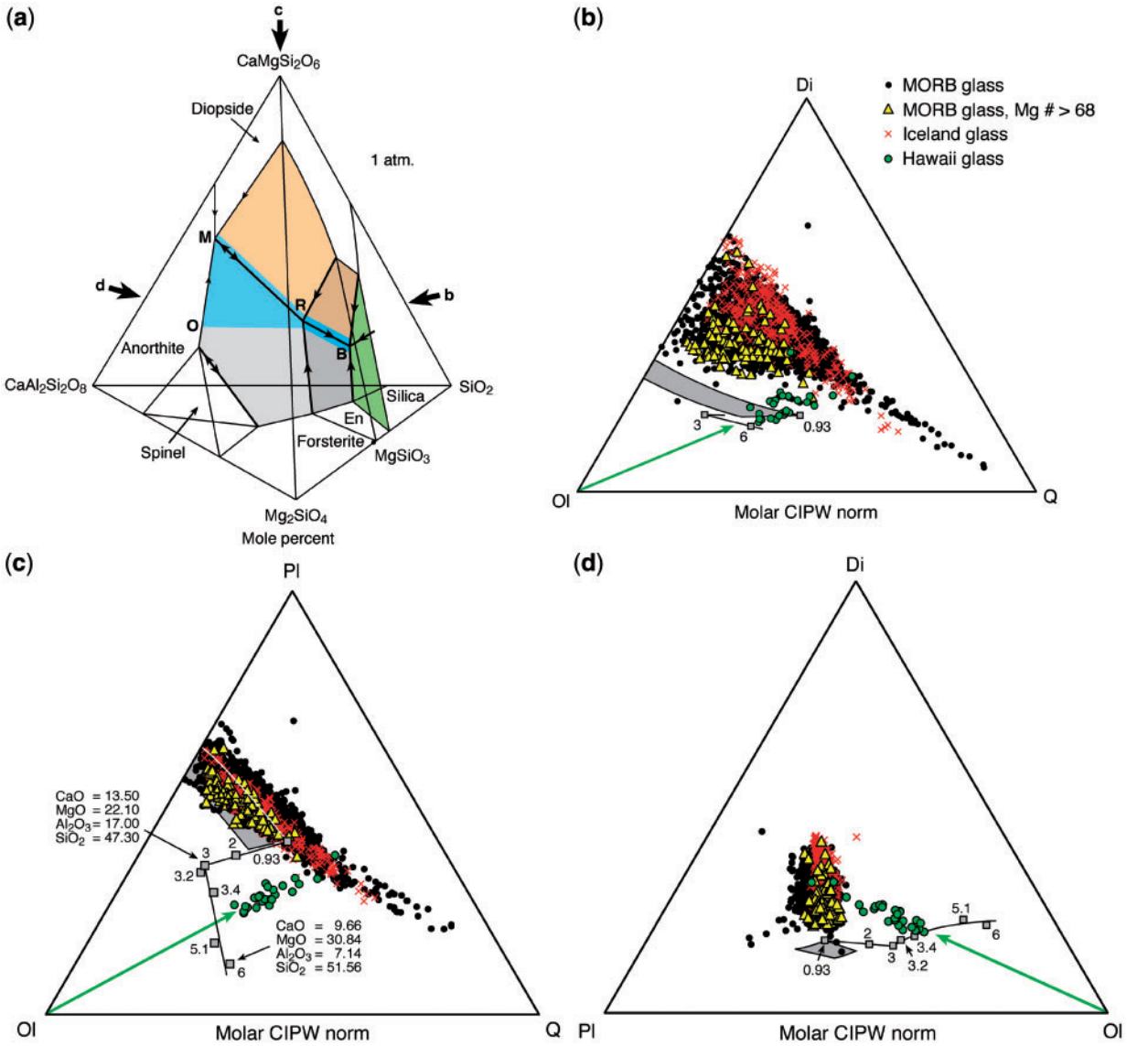

Fig. 1. Liquidus phase relations in the tetrahedral Mg_2SiO_4–$CaMgSi_2O_6$–$CaAl_2Si_2O_8$–SiO_2 system at 1 atm, modified after Presnall (1999). [For data sources, see Presnall (1999).] Bold liquidus univariant boundary lines are within the tetrahedron and fine liquidus univariant boundary lines are on the faces. Arrows on boundary lines where three crystalline phases are in equilibrium with liquid indicate directions of decreasing temperature. Complex natural glass compositions are reduced to the four components of this system using the CIPW algorithms given by Presnall *et al.* (2002, fig. 6 caption). The blue M-O-R-B field indicates the field of model mid-ocean ridge basalt glass compositions. Bold black arrows in (a) indicate viewing directions for diagrams (b), (c) and (d). For example, in (b), the view is toward the $CaAl_2Si_2O_8$ apex and phase boundaries and glass compositions are projected from the $CaAl_2Si_2O_8$ apex onto the $CaMgSi_2O_6$–SiO_2–Mg_2SiO_4 face. The gray trapezoidal area in (b)–(d) is an approximation of the plagioclase–spinel lherzolite solidus in the CaO–MgO–Al_2O_3–SiO_2–Na_2O–FeO system. This solidus extends from 0·93 to ~1·5 GPa. The white line in (c) is the boundary of the gray plagioclase–spinel lherzolite solidus surface hidden underneath the data points. Connected gray squares show the trace of near-solidus liquids for the spinel lherzolite (0·93–3 GPa) and garnet lherzolite (3–6 GPa) solidus in the CaO–MgO–Al_2O_3–SiO_2 system. Diagram (c) shows compositions of lherzolite solidus liquids in the CaO–MgO–Al_2O_3–SiO_2 system at 3 GPa (Milholland & Presnall, 1998) and 6 GPa (Table 1).

CMAS tetrahedron (Fig. 1) it has been demonstrated that crystallization paths for model tholeiitic basalt magma compositions at 1 atm pressure in this system correspond closely to crystallization paths for natural MORB and Hawaiian glass compositions that have crystallized at very low pressures within the volcanic edifice (Presnall, 1999, fig. 11; Presnall *et al.*, 2002, figs 11 and 12). To address MORB and Hawaiian *P-T* conditions of magma extraction with greater precision, we use extensions of the CMAS phase relations at pressures up to 6 GPa (Weng, 1997;

Weng & Presnall, 2001; Dalton, J. A., unpublished) and with the additional components, Na_2O and FeO (CMASNF) (Walter & Presnall, 1994; Gudfinnsson & Presnall, 2000; Presnall *et al.*, 2002; Presnall & Gudfinnsson, 2008). When plotting the compositions of chemically complex natural basalt glasses for comparison with the CMAS and CMASNF phase relations, we use the algorithm given by Presnall *et al.* (2002). For tholeiitic basalt compositions (those within the tetrahedron olivine–diopside–enstatite–quartz), this algorithm gives the molar equivalent of the classical CIPW norm and includes all the oxides of a normal chemical analysis. This allows the full chemistry of natural magma compositions to be compared in a meaningful way with the simplified model-system phase diagrams (Fig. 1).

Role of volatiles in mantle melting

Carbon has a unique behavior that gives it a critically important role in producing melt in the low-velocity zone. At upper mantle P–T conditions of <6 GPa, 1200°C, carbon has a maximum solubility in mantle silicate minerals of <~13 ppm (Keppler *et al.*, 2003; Shcheka *et al.*, 2006). Because of this nearly complete insolubility and the low melting temperatures of carbonates relative to those of silicates, the silicate mantle can be considered, to first order, as an inert crucible for the production of low-temperature carbonate-rich melts (bold continuous line in Fig. 2a and b) (Wyllie & Huang, 1975*a*, 1975*b*, 1976; Eggler, 1976, 1978; Wyllie, 1978; Gudfinnsson & Presnall, 2005; Presnall & Gudfinnsson, 2005). For natural carbonated lherzolite, solidus temperatures are reduced from ~1250°C at 1·2–1·5 GPa to ~1000°C at ~2 GPa (Falloon & Green, 1989) (Fig. 2a and b), a result generally consistent with the recent study of Dasgupta & Hirschmann (2006) over a wider pressure range.

Presnall & Gufinnsson (2005) showed that observed amounts of H_2O in nominally anhydrous lherzolite minerals are much smaller than the aggregate maximum solubility of H_2O in these minerals. More recent data (Hauri *et al.*, 2006; Grant *et al.*, 2007*a*, 2007*b*) have not changed this observation. Mierdel *et al.* (2007) argued that a minimum in the bulk solubility of H_2O at ~5 GPa might be the cause of the oceanic low-velocity zone. However, their minimum solubility is ~700 ppm, roughly twice the maximum bulk concentration of H_2O observed in natural mantle minerals proportioned to approximate a garnet lherzolite (Presnall & Gudfinnsson, 2005; Table 1). This indicates that all of the H_2O in the oceanic upper mantle can be stored in nominally anhydrous phases. Although Green *et al.* (2010) suggested pargasite as a hydrous phase for storage of H_2O in the mantle, the large amount of unused solubility of H_2O in nominally anhydrous phases indicates that separate hydrous phases such as pargasite would not usually form. Therefore, we argue that H_2O is not the cause of melting in the low-velocity zone in regions

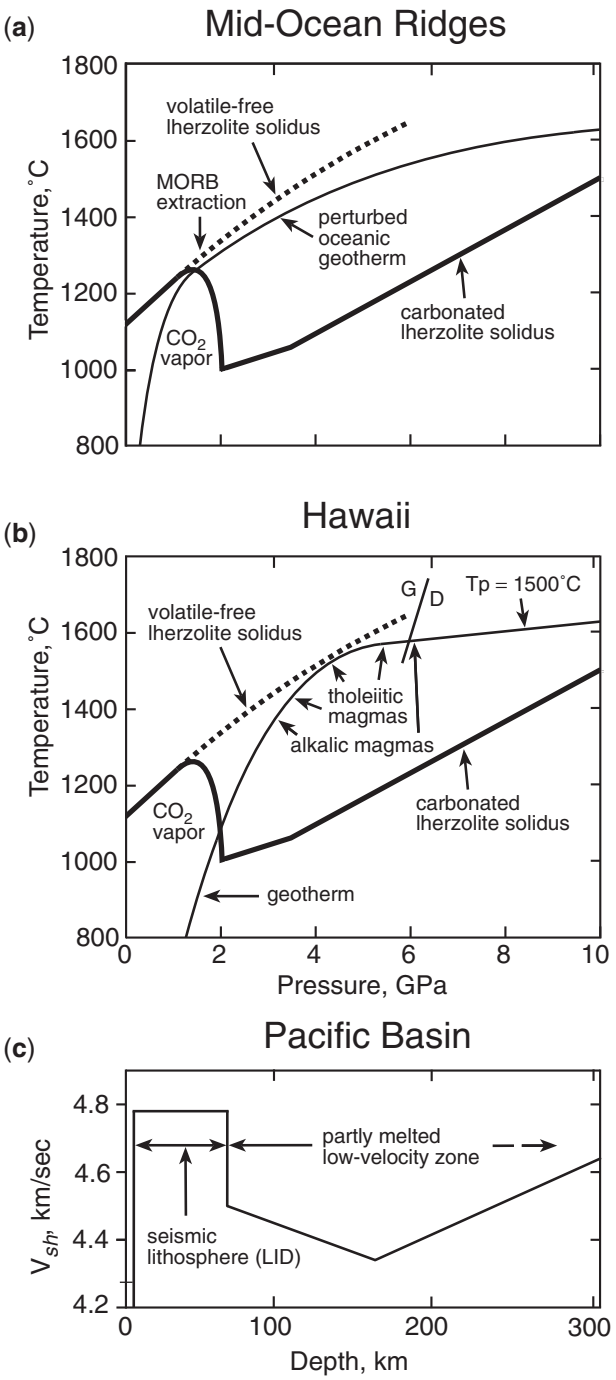

Fig. 2. Comparison of horizontal shear velocities (V_{sh}) for a SW–NE section across the Pacific Basin (Tan & Helmberger, 2007) (c) with solidus curves and geotherms for Hawaii (b) and mid-ocean ridges (a). G/D is the graphite–diamond transition (Bundy *et al.*, 1961). The geotherm for Hawaii assumes a 1500°C adiabat. The natural volatile-free lherzolite solidus (bold dashed line) is constrained at 5 GPa, 1600°C by the determination of Lesher *et al.* (2003). The natural carbonated lherzolite solidus (bold continuous line) is from Falloon & Green (1989) and Dasgupta & Hirschmann (2006). T_p is potential temperature. The P–T space between these two curves is a region of olivine + orthopyroxene + clinopyroxene + garnet + carbonate-bearing melt. The slight change in slope of the carbonated lherzolite solidus at 3·5 GPa is caused by intersection of the solidus with the dolomite–magnesite transition (Dalton & Presnall, 1998).

Table 1: Electron microprobe analyses of near-solidus melt fractions in CMAS in equilibrium with a garnet lherzolite mineralogy at 3–6 GPa

Temperature (°C):	1568	1595	1615	1830	1945
Pressure (GPa):	3·0	3·2	3·4	5·1	6·0
Duration (h):	72·0	24·0	24·0	0·5	0·5
Apparatus:	PC	PC	PC	MA	MA
Source/run no.:	CSM	32.6.2	34.6.3	YHW	JAD
Glass					
CaO	13·50	13·29	12·7	11·18	9·66
MgO	22·10	22·71	23·81	29·07	30·84
Al_2O_3	17·00	15·96	14·46	9·22	7·14
SiO_2	47·30	47·05	48·18	50·55	51·56
Total	99·90	99·01	99·15	100·02	99·20
Forsterite					
CaO	n.a.	n.a.	n.a.	0·40	0·38
MgO	n.a.	n.a.	n.a.	56·41	56·25
Al_2O_3	n.a.	n.a.	n.a.	0·28	0·21
SiO_2	n.a.	n.a.	n.a.	42·21	43·23
Total				99·30	100·07
Enstatite					
CaO	2·83	2·77	2·88	2·33	2·79
MgO	32·90	34·24	35·21	36·20	36·49
Al_2O_3	10·60	8·83	6·83	4·37	2·16
SiO_2	53·60	54·07	55·34	56·37	58·82
Total	99·90	99·91	100·19	99·27	100·27
Diopside					
CaO	13·80	13·02	13·28	9·21	11·75
MgO	23·70	25·36	25·90	30·77	28·86
Al_2O_3	10·90	9·55	8·19	3·83	2·41
SiO_2	51·40	51·84	52·68	55·66	57·20
Total	99·80	99·77	100·05	99·47	100·22
Garnet					
CaO	5·43	5·41	5·32	3·74	3·92
MgO	25·20	25·14	25·29	27·00	27·47
Al_2O_3	25·20	24·72	24·82	24·24	23·15
SiO_2	44·20	44·22	44·54	44·51	46·36
Total	100·03	99·49	99·97	99·49	100·90

PC, piston-cylinder; MA, multianvil. CSM, Milholland & Presnall (1998); YHW, Weng (1997); JAD, J. A. Dalton (unpublished data); n.a., not analysed.

away from subduction zones. However, given the existence of melt caused by CO_2, some of the H_2O that would otherwise exist in the nominally anhydrous phases would partition into the melt.

As temperatures increase above the melting temperatures for carbonates, the approximation of the lherzolitic mantle as a crucible for carbonatitic melts gradually breaks down, and the carbonate–silicate melts become progressively more siliceous. For a given pressure and bulk composition (including CO_2) in the temperature interval between the carbonated and carbonate-free lherzolite solidus curves (Fig. 2b; see also Gudfinnsson & Presnall, 2005), increasing temperature causes the liquid proportion and the proportions of MgO, Al_2O_3, and SiO_2 in the liquid to increase as CaO and CO_2 decrease. Thus, for low temperatures at and just above the carbonated lherzolite solidus, the initial melts are carbonatitic. As temperature increases at constant pressure, the melt compositions change gradationally to simplified approximations of alkalic melts (low in SiO_2), and finally to tholeiitic melts at and immediately below the volatile-free lherzolite solidus. At pressures $> \sim 1{\cdot}5$ GPa and over the entire P–T interval between the volatile-free and carbonated lherzolite solidus curves, all of these liquids of various composition are in equilibrium with the four important minerals of lherzolite: olivine, enstatite, diopside, and an aluminous phase (spinel or garnet). The existence of this broad P–T region between the volatile-free and carbonated lherzolite solidus curves, with its very wide range of magma types, all of which are in equilibrium with a lherzolitic (olivine + orthopyroxene + clinopyroxene + garnet) mineral assemblage (Gudfinnsson & Presnall, 2005), provides the framework used here for understanding the wide range of magma compositions that exist at different depths in the oceanic low-velocity zone and erupted in the ocean basins.

EVIDENCE FOR AN OLIVINE-BEARING SOURCE FOR HAWAIIAN MAGMAS

Hauri (1996) has claimed that Hawaiian lavas, especially those at Koolau, are so high in SiO_2 that olivine cannot be in the source. Also, Sobolev *et al.* (2005) have argued that 40–60% of Hawaiian lavas come from a source that has no olivine. Sobolev *et al.* (2005) based their claim on the observation that Hawaiian tholeiites have high MgO, SiO_2, and Ni, and argued that this combination of enrichments is not consistent with melts produced from a source containing olivine. They also argued that Hawaiian tholeiites with high SiO_2 (>47%) are possible only for high degrees of melting. They noted that the observed high concentrations of Ni in Hawaiian magmas can be produced only if the melts have MgO > 22 wt %, which would decrease the Ni partition coefficient sufficiently to allow the observed high Ni concentrations.

Figure 1 shows that the olivine-controlled crystallization trend for Hawaii discovered by Clague *et al.* (1995) indicates magma extraction at ~4–5 GPa in the garnet lherzolite stability field. In the CMAS system (Fig. 1c and Table 1) initial melts at the smallest melt fractions directly

at the solidus and in equilibrium with a garnet lherzolite mineralogy (olivine + enstatite + diopside + garnet) increase in SiO_2 from 47·30 to 51·56 wt % as pressure increases from 3 to 6 GPa. For these same conditions, MgO in the melt increases from 22·10 to 30·84 wt %. Thus, melts with high Ni and SiO_2 do not indicate the absence of olivine in the source. Instead, melts extracted from a garnet lherzolite mineralogy at ~4–5 GPa yield magmas that are high in both MgO and SiO_2, exactly the features observed by Hauri (1996) and Sobolev *et al.* (2005) and indicated by Sobolev *et al.* (2005) to be necessary for the observed high Ni in Hawaiian tholeiitic magmas. The reason for the simultaneous increase in both MgO and SiO_2 with increasing pressure of melt extraction is the abrupt change in the compositional trajectory of melt compositions vs pressure when the mineral assemblage at the solidus changes from spinel lherzolite to garnet lherzolite at 3 GPa (Table 1 and Fig. 1b–d).

The close consistency between the olivine-controlled glass compositions of Clague *et al.* (1995) and the phase relations (Fig. 1b–d) indicates a source with a garnet lherzolite mineralogy. However, the phase relations do not constrain the proportions of these minerals in the source. For example, the source could be a garnet pyroxenite that contains significant amounts of clinopyroxene, orthopyroxene, and garnet, but only a modest amount of olivine, a rock with many similarities to the olivine-bearing garnet pyroxenite xenoliths at Salt Lake Crater, Hawaii. However, these particular xenoliths (Keshav *et al.*, 2007) have Fe/Mg ratios that are too high to be the source of Hawaiian tholeiites.

PRESSURE–TEMPERATURE CONDITIONS OF HAWAIIAN VOLCANISM

The classic Hawaiian sequence of volcanism (Clague & Dalrymple, 1987) starts with small volumes of alkalic lavas. This is followed by voluminous shield-building tholeiitic lavas that make up the main bulk of the volcano and then a late cap of alkalic lavas. Volcanic activity sometimes stops at this stage. However, for East Maui, Koolau, Kauai, and Niihau, a period of quiescence lasting from 0·25 to 2·5 Myr is followed by the formation of small and short-lived post-erosional vents on the volcano flanks that erupt more strongly alkalic lavas.

Early alkalic basalts

For the P–T conditions of melt extraction of the early Hawaiian alkalic lavas, we use the recent estimates of Sisson *et al.* (2009, fig. 14) for early basanite–nephelinite glasses from Kilauea, the North Arch volcanic field, and the Honolulu Volcanic Series. These estimates, all close to 3 GPa, 1350°C, are consistent with P–T determinations for spinel lherzolite xenoliths from Hawaii (I. D. MacGregor, personal communication) and the mature Hawaiian geotherm (Fig. 2b) based on the seismic constraint of maximum melting at ~120–160 km depth.

Tholeiitic basalts

Hawaiian tholeiites show an initial olivine-controlled differentiation trend and a subsequent trend produced by crystallization of olivine + plagioclase + diopside. Both trends are produced by low-pressure crystallization and the latter trend overlaps the low-pressure crystallization trend of MORB. In Fig. 1, the starting point for olivine-controlled crystallization of the Puna Ridge tholeiitic glasses of Kilauea volcano (Clague *et al.*, 1995) is close to the trend of CMAS near-solidus liquids in equilibrium with olivine, enstatite, diopside, and garnet in all three projections at ~4–5 GPa (Fig. 1b–d). For this pressure range, the model-system temperatures would be ~1450–1560°C for natural compositions, conditions that are consistent with the natural lherzolite solidus temperature of 1600°C at 5 GPa (Lesher *et al.*, 2003). This is the approximate P–T condition for melt extraction of the Puna Ridge tholeiites. The glass composition at the most magnesian end of the Puna Ridge olivine-controlled trend (Fig. 1b–d) is close to the experimental trend of melt compositions in equilibrium with a model lherzolite mineralogy. This implies very little olivine crystallization for this glass, and suggests an explosive eruption from ~140 km depth, which is consistent with recovery of only very small glass fragments (Clague *et al.*, 1995).

Dunite xenoliths at Hawaii provide additional support for low-pressure olivine-controlled crystallization, and therefore deep melt extraction. In the central and deeply eroded core of Koolau volcano, olivine crystals in these xenoliths extend to compositions that are too Fe-rich ($Fo_{82·6}$–$Fo_{89·7}$) to be residues from partial melting. Instead, they must have settled during shallow olivine-controlled crystallization of magnesian melts produced during the main shield-building stage of Koolau (Sen & Presnall, 1986). This concentration of olivine-rich xenoliths is consistent with the high gravity anomaly centered on Koolau (Strange *et al.*, 1965). The existence of similar xenoliths at Hualalai (Chen *et al.*, 1992), Loihi (Clague, 1988), and Mauna Kea (Atwill & Garcia, 1985) indicates a consistent pattern of tholeiitic melt extraction at ~3·5–5 GPa and low-pressure olivine-controlled crystallization of these magmas.

Late alkalic lavas

The most complete data on the late alkalic lavas that characterize the Hawaiian volcanoes (Macdonald & Katsura, 1964) are from the HSDP2 drill core on the flank of Mauna Kea volcano; Stolper *et al.* (2004), however, found no clear indicators of the P–T conditions of melt extraction. The phase relations (Fig. 2b and Gudfinnsson &

Presnall, 2005) show that if the depth of melt extraction continues to increase along the adiabatic part of the geotherm at pressures > ~5 GPa, the magmas will change from tholeiitic to alkalic (lower SiO_2) compositions. Given the even more extreme pressures required for the final post-erosional lavas, we suggest a pressure range of 5–6 GPa for the late alkalic lavas.

Post-erosional lavas

The lava at a small post-erosional crater, Salt Lake Crater, on the flank of Koolau volcano contains garnet pyroxenite xenoliths (Keshav *et al.*, 2007) that have nanodiamonds (Wirth & Rocholl, 2003; Frezotti & Peccerillo, 2007). Intersection of the oceanic geotherm (Fig. 2b) with the graphite–diamond transition curve (Bundy *et al.*, 1961) indicates melt extraction at P–T conditions >6 GPa, 1570°C. The presence of nanodiamonds is consistent with the occurrence of garnets in these same xenoliths that contain exsolved orthopyroxene in their cores. These garnets have been interpreted as originally majoritic garnets formed at 6–9 GPa (Keshav & Sen, 2001).

MAGMA STRATIGRAPHY IN THE MATURE LOW-VELOCITY ZONE

Anderson and Sammis (1970) were the first to recognize that the low-velocity zone is a region of partial melting. We use the system CaO-MgO-Al_2O_3-SiO_2-CO_2 (Gudfinnsson & Presnall, 2005; Fig. 1) as a guide to the melting behavior of natural carbonated lherzolite in the low-velocity zone. This is justified by the nearly identical form of the solidus of a natural carbonated lherzolite determined by Falloon & Green (1989) to the carbonated lherzolite solidus in the five-component model system, except that temperatures are higher in the model system. The data of Gudfinnsson & Presnall (2005) indicate that in the region between the volatile-free and carbonated lherzolite solidus curves (Fig. 2b), melt compositions in equilibrium with a lherzolitic mantle source increase in MgO, Al_2O_3, and SiO_2 and decrease in CaO and CO_2 as temperature increases isobarically. Along the geotherm, melts at ~140–160 km depth are tholeiitic and high in SiO_2. Melts along the geotherm at both lesser and greater depths are progressively lower in SiO_2 and therefore progressively more alkalic. In the low-velocity zone, these changing P–T conditions along the geotherm indicate stratification of equilibrium magma types. High melt-fraction tholeiitic magmas occur in the middle of the low-velocity zone where the geotherm grazes the volatile-free solidus at depth of ~140–160 km. At both lower and higher pressures where the geotherm curves away from the volatile-free solidus, alkalic magmas produced at low to moderate melt fractions occur. At the extreme upper and lower boundaries of the low-velocity zone, carbonatitic magmas occur at both low and high pressures where the geotherm approaches the carbonated lherzolite solidus (Fig. 2b); however, these melts would be very small in volume and unlikely to be observed at the surface.

Mature areas of the Pacific Basin (ages > ~50 Ma) have a uniform depth of minimum vertical shear-wave velocity (V_{sv}) and maximum shear-wave anisotropy of ~140–150 km (Nishimura & Forsyth, 1989; Ekström, 2000; Ritzwoller *et al.*, 2004; Maggi *et al.*, 2006; Kustowski *et al.*, 2008; Nettles & Dziewonski, 2008). The existence of this low-velocity zone has been known for more than 50 years (Gutenberg, 1959; Anderson, 1966) and the depth of maximum velocity reduction has not changed with more recent studies. Figure 2c shows the results of a pure-path study for a line from Tonga–Fiji to southern California (Tan & Helmberger, 2007), which is consistent with seismic tomography data for ages > ~50 Ma (Maggi *et al.*, 2006). Directly beneath (Li *et al.*, 2000) and just SW of the island of Hawaii (Laske *et al.*, 2007), the lowest shear velocity is centered at ~150 km depth, in excellent agreement with the results of Tan & Helmberger (2007) and other data for the mature Pacific Basin. This agreement indicates that temperatures beneath Hawaii are indistinguishable from those beneath lithosphere of a similar age throughout the Pacific Basin. Therefore, Hawaii cannot be a plume. Instead, it appears to be the world's best sampling of magmas in the low-velocity zone.

MAGMA EXTRACTION FROM THE MATURE LOW-VELOCITY ZONE

The sequence of Hawaiian magmas produced at each volcano is identical to the magma stratigraphy indicated by the phase relations in the pressure range of the low-velocity zone. This consistency applies to the relative volumes of the alkalic and tholeiitic magmas as well as their compositions. We interpret this to indicate that each Hawaiian volcano extracts melts through a fracture in the lithospheric lid (LID) and extracts the locally available melt at progressively greater depths until the deeper part of the low-velocity zone is reached and the supply of magma is exhausted. No decompression melting is needed; the sequence and relative volumes of erupted magma compositions at Hawaiian volcanoes match the equilibrium magma stratigraphy vs depth in the low-velocity zone; that is, early small amounts of alkalic basalts from ~3 GPa (~100 km), voluminous tholeiitic basalts from ~4–5 GPa (~120–160 km), small volumes of late alkalic basalts from ~5–6 GPa (~170 km), and, for some volcanoes, post-erosional alkalic basalts from >~6 GPa (>~180 km), as discussed above. The observed extinction of each Hawaiian volcano is consistent with extraction of melt from progressively greater depths that stops as the lower boundary of the LVZ is approached and the melt

fraction becomes too small for extraction. Each volcano ends its activity in turn as eruptive activity migrates to progressively younger volcanoes to the SE where melts are available at shallower depths. The possibility of inclined melt lenses in the low-velocity zone caused by shear between the LID and the unmelted mantle directly below the LVZ (Holtzman *et al.*, 2003, 2010; Katz *et al.*, 2006) would facilitate extraction of melt. This could also contribute to partial isolation of each successive inclined melt layer and deeper penetration and exhaustion of melt from greater depths in the low-velocity zone.

A standard mechanism for producing mantle melting is adiabatic decompression. When the idea of ascending hot mantle plumes was first introduced (Morgan, 1971, 1972), decompression melting and eruption of lavas at the surface was considered to be an expected consequence—hence, the easy acceptance of localities with high lava production, such as Hawaii and Iceland, as hot mantle plumes. However, given the broad depth range of melting in the oceanic low-velocity zone, volcanism does not require decompression melting. It is necessary only to fracture the LID to provide an escape path for magma that already exists. A strong and perhaps dominant force that would drive the escape of magma is caused by the unusual shape of the carbonated lherzolite solidus (Fig. 2a and b), which shows a steep drop in temperature at the approximate depth of the bottom of the LID. The close match of the depth for this temperature drop with the depth for beginning of melting strongly suggests that CO_2 is the cause of this seismic discontinuity.

Pressure release caused by fracturing of the LID would allow CO_2 dissolved in the melt at the top of the LVZ to convert to vapor, which would assist the escape of melt to the surface. In support of this mechanism, CO_2 emissions from the summit of Kilauea volcano average ~4900 metric tons per day (Hager *et al.*, 2008) and have reached as much as ~9000 metric tons per day (Gerlach *et al.*, 2002). Also, Dzurisin *et al.* (1995) have documented the violent phreatomagmatic eruption of the Uwekahuna Ash, which occurred at Kilauea between 2800 and 2100 years ago. This has a thickness of up to 5 m and covers an area of ~420 km^2. The cause of this explosive eruption is unknown, but sudden pressure-release conversion of CO_2 to vapor is the most likely explanation. In addition, Clague *et al.* (2003*a*, 2003*b*) documented pyroclastic deposits at Loihi Seamount, Hawaii, and submarine strombolian eruptions on the Gorda Ridge.

The idea of a propagating fracture to explain the Hawaiian chain of volcanoes was first proposed by Dana (1849), a model advocated in the more recent literature by Fiske & Jackson (1972), Jackson *et al.* (1972, 1975), and Jackson & Shaw (1975). Recently, Natland & Winterer (2005) have called on fissures to account for the very large number of volcanoes in the western Pacific, many of which define linear trends strongly suggestive of fracture control. Fracture control of volcanism at Hawaii is consistent with the finding (Stuart *et al.*, 2007) that tension exists perpendicular to the Hawaiian island chain. Also, relocations of earthquakes beneath Kilauea volcano indicate depths up to 55 km along a roughly vertical and planar fracture system that extends through most of the LID and has a NW–SE orientation (Wolfe *et al.*, 2003, fig. 2). For a vertical section perpendicular to the Hawaiian chain just SW of Maui, the depth to the upper boundary of the partly melted LVZ is ~60–70 km (Laske *et al.*, 2007), which is consistent with the maximum depth of Kilauea earthquakes. Also, they found the minimum shear-wave velocity at a depth of ~140 km, identical to tomographic results for the mature part of the Pacific Basin.

THE PERTURBED MID-OCEAN RIDGE GEOTHERM

Seismic data provide constraints on depths of melting in the upper mantle as mid-ocean ridges are approached. For a ray path along the axis of the East Pacific Rise, Nishimura & Forsyth (1989) and Webb & Forsyth (1998) found the depth of minimum shear-wave velocity at ~60–70 km. Also, seismic tomography indicates that for oceanic crust ages < ~50 Ma, the depth of minimum shear-wave velocity and maximum shear-wave anisotropy decreases with decreasing age (Ekström, 2000; Maggi *et al.*, 2006; Nettles & Dziewonski, 2008). Along the East Pacific Rise, Mid-Indian Ridge, and Mid-Atlantic Ridge, Gu *et al.* (2005, fig. 6a) showed very shallow depths of maximum shear-wave anisotropy at ~50–60 km depth. Also, at 50 km depth, Ritsema *et al.* (2004, fig. 7) showed lower shear-wave velocities along ridges relative to velocities in mature parts of the ocean basins. To satisfy this consistent feature along ridges, the geotherm must have its closest approach to the volatile-free solidus (maximum melt fraction) in the depth range of the lower boundary of the LID, ~65 km (Figs 2a and c). This is consistent with *P-T* conditions of melt extraction of ~1·2–1·5 GPa, 1240–1260°C (Fig. 2a; Presnall *et al.*, 2002), and requires a steepened conductive portion of the ridge geotherm relative to that for mature oceanic mantle (Fig. 2a). It is also consistent with oceanic heat-flow variations vs age (DeLaughter *et al.*, 2005). We (Presnall *et al.*, 2002; Presnall & Gudfinnsson, 2008) have noted that these *P-T* conditions coincide with the maximum temperature conditions for conversion of CO_2 to vapor and have suggested that this may control the observed narrow *P-T* conditions for MORB extraction. The ridge geotherm (Fig. 2a) has been drawn so that *P-T* conditions for a mature oceanic upper mantle are fully recovered at ~250–300 km depth. This depth is approximate and is constrained by the observation that the association of low shear-velocity with the oceanic

ridge system disappears at a depth somewhere between 200 and 350 km (e.g. Ritsema & van Heijst, 2004, fig. 7).

MELTING BEHAVIOR BENEATH YOUNG (<50 MA) OCEANIC LITHOSPHERE

The upper mantle beneath the East Pacific Rise is different from mature Pacific mantle. Nishimura & Forsyth (1989) and Webb & Forsyth (1998) found that a ray path along the axis of the East Pacific Rise shows a depth of minimum V_{sv} of 60–70 km and a depth of maximum shear-wave anisotropy of ~60 km. These seismic results have been confirmed by more recent seismic tomography imaging (Ekström, 2000; Maggi *et al.*, 2006). For progressively older crustal ages to the west, these results showed that this depth increases to about 150 km at ~50 Ma and remains stable at this depth for greater ages. Also, the western side of the East Pacific Rise shows greater electrical conductivity than the eastern side (Conder *et al.*, 2002), which has been interpreted in terms of a larger melt fraction. This interpretation is consistent with experimental data showing that complete melting of crystalline basalt causes electrical conductivity to increase about two orders of magnitude (Presnall *et al.*, 1972).

The seismic data, when combined with the phase relations, require that the geotherm beneath the East Pacific Rise approaches the volatile-free solidus closely at ~60–70 km beneath the East Pacific Rise, but at ~150 km depth at Hawaii. The perturbed geotherm at the ridge axis (Fig. 2a) is consistent with the presence of partly melted mantle in the low-velocity zone that rises, decompresses, and therefore increases its melt fraction dominantly on the west side of the ridge. This rise and enhanced melting owing to decompression shifts the depth range of maximum melting beneath the ridge from ~150 to ~65 km depth. Because the location of the ridge migrates with time, the perturbed geotherm must also migrate, thus producing a stable thermal structure directly at the ridge axis. This stability is consistent with the phase equilibrium constraint of uniformly low-pressure conditions for melt extraction at all mid-ocean ridges, equivalent to depths of ~65 km (Presnall & Gudfinnsson, 2008), an idea suggested very early on by Green & Ringwood (1967), Kushiro (1973) and Presnall *et al.* (1979).

In this model, there is no involvement of the deep mantle beneath the East Pacific Rise, which is consistent with the observation that the 410 and 660 km discontinuities beneath the East Pacific Rise are not perturbed (Melbourne & Helmberger, 2002). As the compositions of MORB glasses globally are very consistent with MORB glass compositions at the East Pacific Rise (Fig. 1b–d), we conclude that the shallow depth of melting at ~65 km applies globally for all mid-ocean ridges.

MID-OCEAN RIDGE BASALTS

In Fig. 1, MORB glass compositions are compared with liquidus phase boundaries in the CMAS system at 1 atm pressure. The tightly packed array of these compositions has the shape of a flattened funnel that closely mimics the M-O-R-B region of Fig. 1a, a correspondence that occurs even though the phase relations are for a system of only four components. This is consistent with a direct comparison between a calculated crystallization path in the CMAS system and the MORB glass array (Presnall, 1999, fig. 11). In the CMAS system, compositional relationships are well modeled, but temperatures are somewhat higher than those for natural compositions. As additional components are added, the model-system temperatures closely approach those of fully complex natural compositions, and the small amounts of these additional components do not significantly change the major-element crystallization trend of the glass compositions. Thus, when all of the major phase are included in the model system, the simplified phase relations are an excellent guide to the crystallization behavior of natural basaltic magmas, even though temperatures for the model system are usually higher. A more comprehensive discussion of the low-pressure crystallization of MORBs is available (Grove *et al.*, 1992), but the simplified version in Fig. 1 captures the essential features. Further support for this claim is provided by experimental studies at 1 atm on the early crystallization stages of primitive natural MORB glass compositions. These studies, summarized by Presnall *et al.* (2002), show that either olivine (usually) or plagioclase (rarely) is the first silicate phase to crystallize, and is followed after a small ($\leq$30°C) temperature interval by the other. This duplicates the early crystallization behavior of model basalts extracted at the plagioclase–spinel lherzolite transition in the CMAS system.

The least-fractionated MORB with Mg-numbers >68 are concentrated toward the low-Di margin of the MORB array (Fig. 1b) and are distributed over a wide range of normative quartz only a short distance from the plagioclase–spinel lherzolite solidus (gray trapezoidal surface in Fig. 1b–d). This wide variation in normative quartz with no indication of olivine-controlled crystallization (which would appear as trends extending from the MORB array toward the olivine apex of the tetrahedron) indicates that MORB are not extracted from the mantle at elevated pressures and temperatures. The array of MORB compositions is the expected result of melt extraction from a heterogeneous lherzolitic mantle at the plagioclase–spinel lherzolite solidus at $P \approx 1{\cdot}2$–$1{\cdot}5$ GPa. The least-fractionated natural MORB glasses show a small separation from the CMASNF solidus surface (Fig. 1b and d), which indicates that even the most primitive MORB glasses have experienced a small amount of olivine + plagioclase crystallization (Presnall *et al.*, 2002; Presnall & Gudfinnsson, 2008)

(Fig. 1). For crystallization experiments on natural compositions, this is consistent with the small (≤30°C) temperature interval between the first appearance of olivine and the appearance of plagioclase as the second crystallizing phase. This small temperature interval is not sufficient to produce a clear trend of either olivine-controlled or plagioclase-controlled crystallization, and is expected from melts extracted in the plagioclase–spinel lherzolite transition interval.

As discussed by Presnall & Gudfinnsson (2008), phase relations for the CMAS and CMASNF systems show that if melts are extracted at P–T conditions >~1·8 GPa, 1280°C, and rise to shallower depths, their compositions would lie within the olivine primary phase volume at low pressure. Cooling of such melts would show initial liquid paths controlled by olivine crystallization. These would appear as linear trends of glass compositions like that found at Hawaii (Fig. 1b–d), which extend from the Mg_2SiO_4 apex toward the low-pressure MORB array. As Fig. 1b–d shows no indication of olivine-controlled crystallization, the P–T conditions for MORB extraction are always <~1·5 GPa, 1280°C and constrain the depth of melt extraction to ~1·2–1·5 GPa (i.e. a depth of ~65 km). This coincides with the depth of minimum shear-wave velocity and maximum shear-wave anisotropy observed at the crest of the East Pacific Rise, which is generally interpreted as the depth of maximum melting.

ICELAND

Figure 1b–d indicates almost complete overlap of Icelandic and other MORB glass compositions, but with Icelandic glasses shifted toward more Di-rich compositions (Fig. 1b and d). This offset and the absence of olivine-controlled crystallization is the expected result of a source that is shifted toward a more fertile composition (Foulger *et al.*, 2005*a*, 2005*b*), with P–T conditions for melt extraction the same as at other locations along ridges, ~1·2–1·5 GPa, 1250–1280°C. Melts with only small differences in composition are expected from a mantle that has significant compositional heterogeneity as long as the heterogeneity is not so extreme that the mineralogy of the source changes (Presnall, 1969). For example, at the plagioclase–spinel lherzolite transition, a source consisting of a mixture of basalt and lherzolite would maintain the same mineralogy as a lherzolite source, but the bulk composition of the source would be shifted toward basalt. This would greatly increase the amount of extractable melt and would slightly change the average composition of the basalts erupted. It would not significantly change the P–T conditions for melt extraction.

Given continuing mantle flow of CO_2-bearing and potentially explosive decompressed melt from the seismic low-velocity zone, volcanism would continue as long as the supply of melt is maintained or until plate-tectonic forces close the fracture used as a magma channel. The vigorous CO_2-driven geyser activity at Iceland indicates that the supply of CO_2 is not currently exhausted. Control of the temperature and pressure of melt extraction by the unusual shape of the carbonated lherzolite solidus (Fig. 2) would keep the P–T conditions for melt extraction at Iceland the same as those at other ridge localities. The complete absence of olivine-controlled crystallization at Iceland (Fig. 1) requires that the P–T conditions for melt extraction are narrow and essentially the same as at all other localities along oceanic ridges (Presnall *et al.*, 2002; Presnall & Gudfinnsson, 2008). No elevated temperatures and pressures of melt extraction that would indicate a hot mantle plume are indicated.

DISCUSSION

Seismic constraints on depths of minimum shear-wave velocity and maximum shear-wave anisotropy (150 km at Hawaii; 65 km at the East Pacific Rise) are in excellent agreement with phase equilibrium constraints for the depths of tholeiitic magma extraction at these two localities. This appears to resolve long-running controversies over the P–T conditions of magma extraction at Hawaii and along the global mid-ocean ridge system. The 65 km depth at ridges closely matches the maximum temperature for conversion of CO_2 to vapor (Fig. 2a) on release of pressure. This conversion, which has been proposed as the control on the P–T conditions of melt extraction at oceanic ridges (Presnall & Gudfinnsson, 2008), is supported by widespread strombolian eruptive features along the Gorda Ridge, Juan de Fuca Ridge, southern East Pacific Rise, northern East Pacific Rise, and Gakkel Ridge (Clague *et al.*, 2003*b*, 2009; Sohn *et al.*, 2008). Strong degassing of CO_2 has also been reported from the Mid-Atlantic Ridge (Javoy & Pineau, 1991; Pineau *et al.*, 2004). Conversion of CO_2 to vapor, as an aid to delivery of melt to the surface, is distinct from the energy source for melting, which comes from upward flow and decompression of mantle source material at pressures greater than ~1·2–1·5 GPa. In contrast to Hawaii, the interpretation of relative eastward and upward flow in the low-velocity zone just west of the East Pacific Rise (Conder *et al.*, 2002) implies enhanced decompression melting of a crystal–liquid mixture that rises from ~150 to ~65 km depth prior to magma extraction at the ridge axis. Such flow is consistent with the tomographic cross-section of Pacific shear-wave anisotropy given by Ekström (2000, plate 2, bottom panel) and the vertical shear-velocity data of Maggi *et al.* (2006, fig. 10). The shallow (~65 km) depth of melt extraction at mid-ocean ridges is identical to the depth of minimum shear velocity (Nishimura & Forsyth, 1989; Webb & Forsyth, 1998).

As many presumed mantle plumes are located on or near mid-oceanic ridges, these plumes should cause local

temperature enhancements of ~250°C (Sleep, 2007). However, the complete absence of olivine-controlled crystallization trends along mid-ocean ridges (Fig. 1b–d) demonstrates that melt extraction always occurs at temperatures significantly lower than the mature oceanic T_p at depths greater than the thermal boundary layer. This occurs because mid-ocean ridge basalts are always extracted from within the thermal boundary layer along a perturbed geotherm. We conclude that upwelling mantle plumes (e.g. at Easter Island) beneath the East Pacific Rise are not required, a result consistent with the absence of Transition Zone topography along the East Pacific Rise (Melbourne & Helmberger, 2002). The globally uniform thermal characteristics of volcanism at mid-ocean ridges, including Iceland, imply that thermally driven upwelling from the lower mantle does not occur beneath any ridge. Our thermal constraint has been developed in detail only for the East Pacific Rise, but this is the most active of all ridges. If hot mantle plumes do not rise from the lower mantle beneath the East Pacific Rise, it is difficult to argue that they rise beneath any other ocean ridge. The enhanced magma production at Iceland, a plume candidate perhaps as strong as Hawaii, does not show any indication of olivine-controlled crystallization. The enhanced magma production is easily understood as the result of mantle heterogeneity.

Wolfe *et al.* (2009) reported a column of low shear velocity that extends to a depth of about 1200 km beneath Hawaii and suggested that this indicates elevated temperatures caused by a plume from the lower mantle. A plume T_p of ~1750°C would be required compared with a mature-ocean T_p of ~1500°C. This would force a pressure for melt extraction that is beyond the range of existing experimental data, but would be ~9–10 GPa (Fig. 2b). No indication of magma extraction at such extreme P–T conditions has ever been found at Hawaii, or anywhere else in the modern volcanic record. We therefore conclude that no hot plume exists at Hawaii, a result consistent with heat-flow data close to Hawaii (DeLaughter *et al.*, 2005; Stein & Von Herzen, 2007).

ACKNOWLEDGEMENTS

We thank Don Anderson, Gillian Foulger, Jim Natland, Mike O'Hara, and Peter Wyllie for very helpful informal reviews and for many stimulating conversations. We thank Karl Gronvold and the Nordic Volcanological Institute for allowing us to use their file of Icelandic basalt glass compositions. We are especially pleased to help honor Peter Wyllie for his pioneering discovery that carbonates at high pressures melt at temperatures far below those of mantle silicates, and for his fundamental contributions to a systematic understanding of carbonate-silicate phase equilibria and their petrological and geodynamical implications.

FUNDING

Financial support was provided by National Science Foundation Grant EAR-0106645.

REFERENCES

Anderson, D. L. (1966). Recent evidence concerning the structure and composition of the Earth's mantle. *Physics and Chemistry of the Earth* **6**, 1–131.

Anderson, D. L. (2010). Hawaii, boundary layers and ambient mantle—geophysical constraints. *Journal of Petrology* (this volume).

Anderson, D. L. & Sammis, C. G. (1970). Partial melting in the upper mantle. *Physics of the Earth and Planetary Interiors* **3**, 41–50.

Atwill, T. M. & Garcia, M. J. (1985). Petrogenesis of ultramafic xenoliths from Mauna Kea: mantle or crust origin. *Transactions of the American Geophysical Union* **66**, 1133.

Breddam, K. (2002). Kistufell: primitive melt from the Iceland mantle plume. *Journal of Petrology* **43**, 345–373.

Bundy, F. P., Bovenkirk, H. P., Strong, H. M. & Wentorf, R. H., Jr (1961). Diamond–graphite equilibrium line from growth and graphitization of diamond. *Journal of Chemical Physics* **35**, 383–391.

Campbell, I. H. & Kerr, A. C. (2007). The Great Plume Debate: Testing the plume theory. *Chemical Geology* **241**, 149–374.

Chen, C.-H., Presnall, D. C. & Stern, R. J. (1992). Petrogenesis of ultramafic xenoliths from the 1800 Kaupulehu flow, Hualalai volcano, Hawaii. *Journal of Petrology* **33**, 163–202.

Clague, D. A. (1988). Petrology of ultramafic xenoliths from Loihi seamount, Hawaii. *Journal of Petrology* **29**, 1161–1186.

Clague, D. A. & Dalrymple, G. B. (1987). The Hawaiian–Emperor volcanic chain, Part 1. Geologic evolution. *US Geological Survey Professional Paper* **1350**, 5–54.

Clague, D. A., Moore, J. G., Dixon, J. E. & Friesen, W. B. (1995). Petrology of submarine lavas from Kilauea's Puna Ridge, Hawaii. *Journal of Petrology* **36**, 299–349.

Clague, D. A., Batiza, R., Head, J. W., III & Davis, A. S. (2003*a*). Pyroclastic and hydroclastic deposits on Loihi Seamount, Hawaii. In: White, J. D. L., Smellie, J. L. & Clague, D. A. (eds) *Explosive Subaqueous Volcanism. American Geophysical Union, Geophysical Monograph* **140**, 73–95.

Clague, D. A., Davis, A. S. & Dixon, J. E. (2003*b*). Submarine Strombolian eruptions along the Gorda mid-ocean ridge. In: White, J. D. L., Smellie, J. L. & Clague, D. A. (eds) *Explosive Subaqueous Volcanism. American Geophysical Union, Geophysical Monograph* **140**, 11–128.

Clague, D. A., Paduan, J. B. & Davis, A. C. (2009). Widespread strombolian eruptions of mid-ocean ridge basalt. *Journal of Volcanology and Geothermal Research* **180**, 171–188.

Conder, J. A., Forsyth, D. W. & Parmentier, E. M. (2002). Asthenospheric flow and asymmetry of the East Pacific Rise, MELT area. *Journal of Geophysical Research* **107**, 2344, doi:10.1029/2001JB000807.

Condomines, M., Grönvold, K., Hooker, P. J., Muehlenbachs, K., O'Nions, R. K., Oskarsson, N. & Oxburgh, E. R. (1983). Helium, oxygen, strontium and neodymium isotopic relationships in Icelandic volcanics. *Earth and Planetary Science Letters* **66**, 125–136.

Courtier, A. M., Jackson, M. G., Lawrence, J. F., Wang, Z., Lee, C.-T. A., Halama, R., Warren, J. M., Workman, R., Xu, W., Hirschmann, M. M., Larson, A. M., Hart, S. R., Lithgow-Bertelloni, C., Stixrude, L. & Chen, W. P. (2007). Correlation of seismic and petrologic thermometers suggests deep thermal

anomalies beneath hotspots. *Earth and Planetary Science Letters* **264**, 308–316, doi:10.1016/j.epsl.2007.10.003.

Dalton, J. A. & Presnall, D. C. (1998). The continuum of primary carbonatitic–kimberlitic melt compositions in equilibrium with lherzolite: Data from the system $CaO–MgO–Al_2O_3–SiO_2–CO_2$ at 6 GPa. *Journal of Petrology* **39**, 1953–1964.

Dana, J. D. (1849). Geology. In: Wilkes, C. (ed.) *United States Exploring Expedition 10. Philadelphia: C. Sherman; with atlas*. New York: Putnam, 756 p.

Dasgupta, R. & Hirschmann, M. M. (2006). Melting in the Earth's deep upper mantle caused by carbon dioxide. *Nature* **440**, 659–662.

DeLaughter, J. E., Stein, C. A. & Stein, S. (2005). Hotspots: A view from the swells. In: Foulger, G. R., Natland, J. H., Presnall, D. C. & Anderson, D. L. (eds) *Plates, Plumes, and Paradigms. Geological Society of America, Special Papers* **388**, 257–278.

Dzurisin, D., Lockwood, J. P., Casaevall, T. J. & Rubin, M. (1995). The Uwekahuna ash member of the Puna basalt: product of violent phreatomagmatic eruptions at Kilauea volcano, Hawaii, between 2800 and 2100 ^{14}C years ago. *Journal of Volcanology and Geothermal Research* **66**, 163–184.

Eggler, D. H. (1976). Does CO_2 cause partial melting in the low-velocity layer of the mantle? *Geology* **4**, 69–72.

Eggler, D. H. (1978). The effect of CO_2 upon partial melting of peridotite in the system $Na_2O–CaO–Al_2O_3–MgO–SiO_2–CO_2$ to 35 kb, with an analysis of melting in a peridotite–$H_2O–CO_2$ system. *American Journal of Science* **278**, 305–343.

Ekström, G. (2000). Mapping the lithosphere and asthenosphere with surface waves: Lateral structure and anisotropy. In: Richards, M. A., Gordon, R. G. & van der Hilst, R. D. (eds) *The History and Dynamics of Global Plate Motions. American Geophysical Union, Geophysical Monograph* **121**, 239–254.

Falloon, T. J. & Green, D. H. (1989). The solidus of carbonated, fertile peridotite. *Earth and Planetary Science Letters* **94**, 364–370.

Falloon, T. J., Green, D. H. & Danyushevsky, L. V. (2005). Crystallization temperatures of tholeiite parental liquids: Implications for the existence of thermally driven mantle plumes. In: Foulger, G. R., Natland, J. H., Presnall, D. C. & Anderson, D. L. (eds) *Plates, Plumes, and Paradigms. Geological Society of America, Special Papers* **388**, 235–260.

Falloon, T. J., Danyushevsky, L. V., Ariskin, A., Green, D. H. & Ford, C. E. (2007). The application of olivine geothermometry to infer crystallization temperatures of parental liquids: Implications for the temperature of MORB magmas. *Chemical Geology* **241**, 207–233.

Fiske, R. F. & Jackson, E. D. (1972). Orientation and growth of Hawaiian volcanic rifts: The effect of regional structure and gravitational stresses. *Proceedings of the Royal Society of London, Series A* **329**, 299–326.

Foulger, G. R., Natland, J. H. & Anderson, D. L. (2005*a*). Genesis of the Iceland melt anomaly by plate tectonic processes. In: Foulger, G. R., Natland, J. H., Presnall, D. C. & Anderson, D. L. (eds) *Plates, Plumes, and Paradigms. Geological Society of America, Special Papers* **388**, 595–625.

Foulger, G. R., Natland, J. H. & Anderson, D. L. (2005*b*). A source for Icelandic magmas in remelted Iapetus crust. *Journal of Volcanology and Geothermal Research* **141**, 23–44.

Foulger, G. R., Natland, J. H., Presnall, D. C. & Anderson, D. L. (2005*c*). *Plates, Plumes, and Paradigms. Geological Society of America, Special Papers* **388**.

Foulger, G. R. & Jurdy, D. M. (2007). *Plates, Plumes and Planetary Processes. Geological Society of America, Special Papers* **430**.

Frezotti, M.-L. & Peccerillo, A. (2007). Diamond-bearing COHS fluids in the mantle beneath Hawaii. *Earth and Planetary Science Letters* **262**, 273–283.

Gerlach, T. M., McGee, K. A., Elias, T., Sutton, A. J. & Douglas, M. P. (2002). Carbon dioxide emission rate of Kilauea volcano: Implications for primary magma and the summit reservoir. *Journal of Geophysical Research—Solid Earth* **107(B9)**, 2189, doi:10.1029/2001JB000407.

Grant, K. J., Brooker, R. A., Kohn, S. C. & Wood, B. J. (2007*a*). The effect of oxygen fugacity on hydroxyl concentrations and speciation in olivine: Implications for water solubility in the upper mantle. *Earth and Planetary Science Letters* **261**, 217–229.

Grant, K. J., Ingrin, J., Lorand, J. P. & Dumas, P. (2007*b*). Water partitioning between mantle minerals from peridotite xenoliths. *Contributions to Mineralogy and Petrology* **154**, 15–34.

Green, D. H. & Falloon, T. J. (2005). Primary magmas at mid-ocean ridges, 'hotspots,' and other intraplate settings: Constraints on mantle potential temperatures. In: Foulger, G. R., Natland, J. H., Presnall, D. C. & Anderson, D. L. (eds) *Plates, Plumes and Paradigms. Geological Society of America, Special Papers* **388**, 217–247.

Green, D. H. & Ringwood, A. E. (1967). The genesis of basaltic magmas. *Contributions to Mineralogy and Petrology* **15**, 103–190.

Green, D. H., Hibberson, W. O., Kovács, I. & Rosenthal, A. (2010). Water and its influence on the lithosphere–asthenosphere boundary. *Nature* **467**, 448–451.

Grove, T. L., Kinzler, R. J. & Bryan, W. B. (1992). Fractionation of mid-ocean ridge basalt (MORB). In: Phipps Morgan, J., Blackman, D. & Sinton, J. M. (eds) *Mantle Flow and Melt Generation at Mid-Ocean Ridges. American Geophysical Union, Geophysical Monograph* **71**, 281–310.

Gu, Y. J., Lerner-Lam, A. L., Dziewonski, A. M. & Ekström, G. (2005). Deep structure and seismic anisotropy beneath the East Pacific Rise. *Earth and Planetary Science Letters* **232**, 259–272.

Gudfinnsson, G. H. & Presnall, D. C. (2000). Melting behavior of model lherzolite in the system $CaO–MgO–Al_2O_3–SiO_2–FeO$ at 0·7–2·8 GPa. *Journal of Petrology* **41**, 1241–1269.

Gudfinnsson, G. H. & Presnall, D. C. (2005). Continuous gradations among primary carbonatitic, kimberlitic, melilititic, basaltic, picritic, and komatiitic melts in equilibrium with garnet lherzolite at 3–8 GPa. *Journal of Petrology* **46**, 1645–1659.

Gurenko, A. A. & Chaussidon, M. (1995). Enriched and depleted primitive melts included in olivine from Icelandic tholeiites: Origin by continuous melting of a single mantle column. *Geochimica et Cosmochimica Acta* **59**, 2905–2917.

Gutenberg, B. (1959). Wave velocities below the Mohorovicic discontinuity. *Geophysical Journal of the Royal Astronomical Society* **2**, 348–351.

Hager, S. A., Gerlach, T. M. & Wallace, P. J. (2008). Summit CO_2 emission rates by the CO_2/SO_2 ratio method at Kilauea Volcano, Hawai'i. *Journal of Volcanology and Geothermal Research* **177**, 875–882.

Hansteen, T. H. (1991). Multi-stage evolution of the picritic Mælifell rocks, SW Iceland: constraints from mineralogy and inclusions of glass and fluid in olivine. *Contributions to Mineralogy and Petrology* **109**, 225–239.

Hauri, E. H. (1996). Major-element variability in the Hawaiian mantle plume. *Nature* **328**, 415–419.

Hauri, E. H., Gaetani, G. A. & Green, T. H. (2006). Partitioning of water during melting of the Earth's upper mantle at H_2O-undersaturated conditions. *Earth and Planetary Science Letters* **248**, 715–734.

Herzberg, C. & Asimow, P. D. (2008). Petrology of some oceanic island basalts: PRIMELT2.XLS software for primary magma calculation. *Geochemistry, Geophysics, Geosystems* **9**, doi:10.1029/2008GC002057.

Herzberg, C. & O'Hara, M. J. (2002). Plume-associated ultramafic magmas of Phanerozoic age. *Journal of Petrology* **43**, 1857–1883.

Herzberg, C., Asimow, P. D., Arndt, N., Niu, Y., Lesher, C. M., Fitton, J. G., Cheadle, M. J. & Saunders, A. D. (2007). Temperatures in ambient mantle and plumes: Constraints from basalts, picrites, and komatiites. *Geochemistry, Geophysics, Geosystems* **8**, doi:10.1029/2006GC001390.

Holtzman, B. K., Groebner, N. J., Zimmerman, M. E., Ginsberg, S. B. & Kohlstedt, D. L. (2003). Stress-driven melt segregation in partially molten rocks. *Geochemistry, Geophysics, Geosystems* **4**, doi:10.1029/2001GC000258.

Holtzman, B. K., Kohlstedt, D. L., Zimmerman, M. E., Heidelback, F., Hiraga, T. & Hustoft, J. (2010). Melt segregation and strain partitioning: Implications for seismic anisotropy and mantle flow. *Science* **301**, 1227–1230.

Jackson, E. D. & Shaw, H. R. (1975). Stress fields in central portions of the Pacific plate: Delineation in time by linear volcanic chains. *Journal of Geophysical Research* **80**, 1861–1874.

Jackson, E. D., Silver, E. A. & Dalrymple, G. B. (1972). Hawaiian–Emperor chain and its relation to Cenozoic circumpacific tectonics. *Geological Society of America Bulletin* **83**, 601–618.

Jackson, E. D., Shaw, H. R. & Bargar, K. E. (1975). Calculated geochronology and stress field orientations along the Hawaiian chain. *Earth and Planetary Science Letters* **26**, 145–155.

Javoy, M. & Pineau, F. (1991). The volatiles record of a 'popping' rock from the Mid-Atlantic Ridge at 14°N: Chemical and isotopic composition of gas trapped in the vesicles. *Earth and Planetary Science Letters* **107**, 598–611, doi:10.1016/0012-821X (91)90104-P.

Kamenetsky, V. S. & Maas, R. (2002). Mantle-melt evolution (dynamic source) in the origin of a single MORB suite: a perspective from magnesian glasses of Macquarie Island. *Journal of Petrology* **43**, 1909–1922.

Katz, R. F., Spiegelman, M. & Holtzman, B. (2006). The dynamics of melt and shear localization in partially molten aggregates. *Nature* **442**, 676–679, doi:10.1038/nature05039.

Keppler, H., Wiedenbeck, M. & Shcheka, S. S. (2003). Carbon solubility in olivine and the mode of carbon storage in the Earth's mantle. *Nature* **424**, 414–416.

Keshav, S. & Sen, G. (2001). Majoritic garnets in Hawaiian xenoliths: preliminary results. *Geophysical Research Letters* **28**, 3509–3512.

Keshav, S., Sen, G. & Presnall, D. C. (2007). Garnet-bearing xenoliths from Salt Lake Crater, Oahu, Hawaii: High-pressure fractional crystallization in the oceanic mantle. *Journal of Petrology* **48**, 1681–1724.

Kushiro, I. (1973). Origin of some magmas in oceanic and circumoceanic regions. *Tectonophysics* **17**, 211–222.

Kustowski, B., Ekström, G. & Dziewonski, A. M. (2008). Anisotropic shear-wave velocity structure of the Earth's mantle: A global model. *Journal of Geophysical Research* **113**, B06306, doi:10.1029/2007JB005169.

Laske, G., Phipps-Morgan, J. & Orcutt, J. A. (2007). The Hawaiian swell pilot experiment—evidence for lithosphere rejuvenation from ocean bottom surface wave data. In: Foulger, G. R. & Jurdy, D. M. (eds) *Plates, Plumes and Planetary Processes. Geological Society of America, Special Papers* **430**, 209–233.

Lee, C.-T. A., Luffi, P., Plank, T., Dalton, H. & Leeman, W. P. (2009). Constraints on the depths and temperatures of basaltic magma generation on Earth and other terrestrial planets using new thermobarometers for mafic magmas. *Earth and Planetry Science Letters* **279**, 20–33.

Lesher, C. E., Pickering-Witter, J., Baxter, G. & Walter, M. (2003). Melting of garnet peridotite: Effects of capsules and thermocouples, and implications for the high-pressure mantle solidus. *American Mineralogist* **88**, 1181–1189.

Li, X., Kind, R., Priestley, K., Sobolev, S. V., Tilmann, F., Yuan, X. & Weber, M. (2000). Mapping the Hawaiian plume conduit with converted seismic waves. *Nature* **405**, 938–941.

Macdonald, G. A. & Katsura, T. (1964). Chemical composition of Hawaiian lavas. *Journal of Petrology* **5**, 82–133.

Maggi, A., Debayle, E., Priestley, K. & Barroul, G. (2006). Multimode surface waveform tomography of the Pacific Ocean: a closer look at the lithospheric cooling signature. *Geophysical Journal International* **166**, 1384–1397.

Melbourne, T. I. & Helmberger, D. V. (2002). Whole mantle shear structure beneath the East Pacific Rise. *Journal of Geophysical Research* **107(B9)**, 2204, doi:10.1029/2001JB000332.

Meyer, P. S., Sigurdsson, H. & Schilling, J.-G. (1985). Petrological and geochemical variations along Iceland's neovolcanic zones. *Journal of Geophysical Research* **90**, 10043–10072.

Mierdel, K., Keppler, H., Smyth, J. R. & Langenhorst, F. (2007). Water solubility in aluminous orthopyroxene and the origin of Earth's asthenosphere. *Nature* **315**, 364–368.

Milholland, C. S. & Presnall, D. C. (1998). Liquidus phase relations in the $CaO–MgO–Al_2O_3–SiO_2$ system at 3·0 GPa: The aluminous pyroxene thermal divide and high pressure fractionation of picritic and komatiitic magmas. *Journal of Petrology* **39**, 3–27.

Morgan, W. J. (1971). Convection plumes in the lower mantle. *Nature* **230**, 42–43.

Morgan, W. J. (1972). Deep mantle convection plumes and plate motions. *AAPG Bulletin* **56**, 203–213.

Natland, J. H. & Winterer, E. L. (2005). Fissure control on volcanic action in the Pacific. In: Foulger, G. R., Natland, J. H., Presnall, D. C. & Anderson, D. L. (eds) *Plates, Plumes, and Paradigms. Geological Society of America, Special Papers* **388**, 687–710.

Nettles, M. & Dziewonski, A. M. (2008). Radially anisotropic shear velocity structure of the upper mantle globally and beneath North America. *Journal of Geophysical Research* **113**, B02303, doi:10.1029/2006JB004819.

Nishimura, C. E. & Forsyth, D. W. (1989). The anisotropic structure of the upper mantle in the Pacific. *Geophysical Journal* **96**, 203–229.

Perfit, M. R., Forari, D. J., Ridley, W. I., Kirk, P. D., Casey, J., Kastens, K. A., Reynolds, J. R., Edwards, M., Desonie, D., Schuster, R. & Paradis, S. (1996). Recent volcanism in the Siqueiros transform fault: picritic basalts and implications for MORB magma genesis. *Earth and Planetary Science Letters* **141**, 91–108.

Pineau, F., Shilobreeva, S., Hekinian, R., Bideau, D. & Javoy, M. (2004). Deep-sea explosive activity on the Mid-Atlantic Ridge near 34°50′N: a stable isotope (C, H, O) study. *Chemical Geology* **211**, 159–175.

Presnall, D. C. (1969). The geometrical analyses of partial fusion. *American Journal of Science* **267**, 1178–1194.

Presnall, D. C. (1999). Effect of pressure on the fractional crystallization of basaltic magma. In: Fei, Y., Bertka, C. M. & Mysen, B. O. (eds) *Mantle Petrology: Field Observations and High Pressure Experimentation: A Tribute to Francis R. (Joe) Boyd. Geochemical Society, Special Publications* **6**, 209–224.

Presnall, D. C. & Gudfinnsson, G. H. (2005). Carbonate-rich melts in the oceanic low-velocity zone and deep mantle. In: Foulger, G. R., Natland, J. H., Presnall, D. C. & Anderson, D. L. (eds) *Plates, Plumes, and Paradigms. Geological Society of America, Special Papers* **388**, 207–216.

Presnall, D. C. & Gudfinnsson, G. H. (2008). Origin of the oceanic lithosphere. *Journal of Petrology* **49**, 615–632.

Presnall, D. C., Simmons, C. L. & Porath, H. (1972). Changes in electrical conductivity of a synthetic basalt during melting. *Journal of Geophysical Research* **77**, 5665–5672.

Presnall, D. C., Dixon, S. A., O'Donnell, T. H. & Dixon, J. R. (1979). Generation of mid-ocean ridge tholeiites. *Journal of Petrology* **20**, 3–35.

Presnall, D. C., Gudfinnsson, G. H. & Walter, M. J. (2002). Generation of mid-ocean ridge basalts at pressures from 1 to 7 GPa. *Geochimica et Cosmochimica Acta* **66**, 2073–2090.

Putirka, K. D. (2005). Mantle potential temperatures at Hawaii, Iceland, and the mid-ocean ridge system, as inferred from olivine phenocrysts: Evidence for thermally driven mantle plumes. *Geochemistry, Geophysics, Geosystems* **6**, doi:10.1029/2005GC000915.

Putirka, K. D. (2008). Excess temperatures at ocean islands: Implications for mantle layering and convection. *Geology* **36**, 283–286.

Putirka, K. D., Perfit, M., Ryerson, F. J. & Jackson, M. G. (2007). Ambient and excess mantle temperatures, olivine thermometry, and active vs. passive upwelling. *Chemical Geology* **241**, 177–206.

Risku-Norja, H. (1985). Gabbro nodules from a picritic pillow basalt, Midfell, SW Iceland. *Nordic Volcanological Institute Professional Paper* **8501**, 32–49.

Ritsema, J. & van Heijst, H. J. (2004). Global transition zone tomography. *Journal of Geophysical Research* **109**, B02302, doi:10.1029/2003JB002610.

Ritzwoller, M. H., Shapiro, N. M. & Zhong, S.-J. (2004). Cooling history of the Pacific lithosphere. *Earth and Planetary Science Letters* **226**, 69–84.

Schiellerup, H. (1995). Generation and equilibration of olivine tholeiites in the northern rift zone of Iceland. A petrogenetic study of the Bláfjall table mountain. *Journal of Volcanology and Geothermal Resources* **65**, 161–179.

Sen, G. H. & Presnall, D. C. (1986). Petrogenesis of dunite xenoliths from Koolau Volcano, Oahu, Hawaii: implications for Hawaiian volcanism. *Journal of Petrology* **27**, 197–217.

Shcheka, S. S., Wiedenbeck, M., Frost, D. J. & Keppler, H. (2006). Carbon solubility in mantle minerals. *Earth and Planetary Science Letters* **245**, 730–742.

Sigurdsson, H. & Sparks, R. S. J. (1981). Petrology of rhyolitic and mixed magma ejecta from the 1875 eruption of Askja, Iceland. *Journal of Petrology* **22**, 41–84.

Sigurdsson, I. A., Steinthórsson, S. & Grönvold, K. (2000). Calcium-rich inclusions in Cr-spinels from Borgarhraun, northern Iceland. *Earth and Planetary Science Letters* **183**, 15–26.

Sisson, T. W., Kimura, J.-I. & Coombs, M. L. (2009). Basanite–nephelinite suite from early Kilauea: carbonated melts of phlogopite–garnet peridotite at Hawaii's leading magmatic edge. *Contributions to Mineralogy and Petrology* **158**, 803–829.

Sleep, N. H. (2007). Origins of the plume hypothesis and some of its implications. In: Foulger, G. R. & Jurdy, D. M. (eds) *Plates, Plumes, and Planetary Processes. Geological Society of America, Special Papers* **430**, 29–45.

Sobolev, A. V., Hofmann, A. W., Sobolev, S. V. & Nikogosian, I. K. (2005). An olivine-free mantle source of Hawaiian shield basalts. *Nature* **434**, 590–597.

Sohn, R. A., Willis, C., Humphris, S., Shank, T. M., Singh, H., Edmonds, H. N., Kunz, C., Hedman, U., Helmke, E., Jakuba, M., Liljebladh, B., Linder, J., Murphy, C., Nakamura, K., Sato, T., Schlindwein, V., Stranne, C., Tausenfreund, M., Upchurch, L., Winsor, P., Jakobsson, M. & Soule, A. (2008). Explosive volcanism on the ultraslow-spreading Gakkel ridge, Arctic Ocean. *Nature* **453**, 1236–1238.

Stein, C. & Von Herzen, R. P. (2007). Potential effects of hydrothermal circulation and magmatism on heat flow at hotspot swells. In: Foulger, G. R. & Jurdy, D. M. (eds) *Plates, Plumes, and Planetary Processes. Geological Society of America, Special Papers* **430**, 261–274.

Steinthórsson, S., Hardarson, B. S., Ellam, R. M. & Larsen, G. (2000). Petrochemistry of the Gjálp (1996) subglacial eruption, Vatnajökull, SE Iceland. *Journal of Volcanology and Geothermal Resources* **98**, 79–90.

Stolper, E., Sherman, S., Garcia, M., Baker, M. & Seaman, C. (2004). Glass in the submarine section of the HSDP2 drill core, Hilo, Hawaii. *Geochemistry, Geophysics, Geosystems* **5**, Q07G15, doi:10.1029/2003GC000553.

Strange, W. E., Woolard, G. P. & Rose, J. C. (1965). An analysis of the gravity field over the Hawaiian Islands in terms of crustal structure. *Pacific Science* **19**, 381–389.

Stuart, W. D., Foulger, G. R. & Barall, M. (2007). Propagation of the Hawaiian–Emperor volcano chain by Pacific plate cooling stress. In: Foulger, G. R. & Jurdy, D. M. (eds) *Plates, Plumes, and Planetary Processes. Geological Society of America, Special Papers* **430**, 497–506.

Tan, Y. & Helmberger, D. V. (2007). Trans-Pacific upper mantle shear velocity. *Journal of Geophysical Research* **112**, B08301, doi:10.1029/2006JB004853.

Trønnes, R. G. (1990). Basaltic melt evolution of the Hengill volcanic system, SW Iceland, and evidence for clinopyroxene assimilation in primitive tholeiitic magmas. *Journal of Geophysical Research* **95**, 15893–15910.

Walter, M. J. & Presnall, D. C. (1994). Melting behavior of simplified lherzolite in the system $CaO–MgO–Al_2O_3–SiO_2–Na_2O$ from 7 to 35 kbar. *Journal of Petrology* **35**, 329–359.

Webb, S. C. & Forsyth, D. W. (1998). Structure of the upper mantle under the EPR from waveform inversion of regional events. *Science* **280**, 1227–1229.

Weng, Y.-H. (1997). Liquidus phase relations for the model basaltic tetrahedron diopside–anorthite–forsterite–quartz in the system $CaO–MgO–Al_2O_3–SiO_2$ at 5·1 GPa, PhD dissertation, University of Texas at Dallas, 76 pp.

Weng, Y.-H. & Presnall, D. C. (2001). The system diopside–forsterite–enstatite at 5·1 GPa: A ternary model for melting of the mantle. *Canadian Mineralogist* **39**, 299–308.

Werner, R. (1994). Struktur und Entstehung subglazialer/subakustrischer Vulkane am Beispiel des Vulkankomplexes Herdubreid/Herdubreidartögl in Island, PhD thesis, Christian-Albrechts-Universität zu Kiel, 153 pp.

Wirth, J. T. & Rocholl, A. (2003). Nanocrystalline diamond from the Earth's mantle underneath Hawaii. *Earth and Planetary Science Letters* **211**, 357–369.

Wolfe, C. J., Okubo, G. & Shearer, P. M. (2003). Mantle fault zone beneath Kilauea Volcano, Hawaii. *Science* **300**, 478–480.

Wolfe, C. J., Solomon, S. C., Laske, G., Collins, J. A., Detrick, R. S., Orcutt, J. A., Bercovici, D. & Hauri, E. H. (2009). Mantle shear-wave velocity structure beneath the Hawaiian hot spot. *Science* **326**, 1388–1390, doi:10.1126/Science.1180165.

Wyllie, P. J. (1978). The effect of H_2O and CO_2 on planetary mantles. *Geophysical Reserch Letters* **5**, 440–442.

Wyllie, P. J. & Huang, W. L. (1975*a*). Influence of mantle CO_2 in the generation of carbonatites and kimberlites. *Nature* **257**, 297–299.

Wyllie, P. J. & Huang, W. L. (1975*b*). Peridotite, kimberlite, and carbonatite explained in the system $CaO–MgO–SiO_2–CO_2$. *Geology* **3**, 621–624.

Wyllie, P. J. & Huang, W. L. (1976). Carbonation and melting reactions in the system $CaO–MgO–SiO_2–CO_2$ at mantle pressures with geophysical and petrological applications. *Contributions to Mineralogy and Petrology* **54**, 79–107.

Yoder, H. S. & Tilley, C. E. (1962). Origin of basalt magmas: an experimental study of natural and synthetic rock systems. *Journal of Petrology* **3**, 342–532.